Self-Sustaining Acoustic Sensor With Programmable Pattern Recognition for Underwater Monitoring

Philipp Mayer, *Student Member, IEEE*, Michele Magno, *Senior Member, IEEE*, and Luca Benini, *Fellow, IEEE*

***Abstract*— Minimizing the power consumption of always-on sensors is crucial for extending the lifetime of battery-operated devices that are required to monitor events continuously and for long periods. This paper proposes a novel programmable μW event-driven acoustic detector featuring "always-on" audio pattern recognition. The event-driven detector detects up to eight programmable spectral–temporal features extracted with a low-power single-channel analog circuit and classifies the features by an onboard microcontroller. The event-driven detector is combined with novel microbial fuel cells (MFCs) to achieve self-sustainability in an underwater scenario. Experimental results demonstrate that the power consumption of the detector is only 26.89 μW during always-on mode, achieving up to 59-dB sound pressure level of sensitivity. High detection accuracy of up to 95.89% in recognizing acoustic patterns has been experimentally verified. Accurate measurements with commercial MFCs demonstrate the capability to achieve self-sustainability in always-on monitoring.**

***Index Terms*— Acoustic sensors, energy harvesting, event-driven sensors, microbial fuel cells (MFCs), underwater monitoring.**

I. Introduction

SMART sensors are gaining popularity in many civilian and military applications, as they embed the capability to directly process data close to the sensor [1], [2]. On the other hand, most sensors today are still "active objects" that continuously consume power to extract useful information from the physical world they are sensing [3]. As a result, these devices require to be constantly supplied by energy sources and the availability of these limits the use of smart sensors in many fields, especially when batteries are used [1], [3]. For instance, smart sensors could have a huge impact on the underwater environment monitoring scenario, but their employment is limited by the battery lifetime as recharging the battery is inconvenient if not impossible [3].

Manuscript received June 11, 2018; revised December 8, 2018; accepted December 10, 2018. This work was supported by the Swiss National Science Foundation projects "MicroLearn: Micropower Deep Learning" under Grant 162524. The Associate Editor coordinating the review process was Dr. Vedran Bilas. *(Corresponding author: Philipp Mayer.)*

P. Mayer is with the Department of Information Technology and Electrical Engineering, ETH Zurich, 8092 Zurich, Switzerland (e-mail: mayerph@iis.ee.ethz.ch).

M. Magno and L. Benini are with the Department of Information Technology and Electrical Engineering, ETH Zurich, 8092 Zurich, Switzerland, and also with the Department of Electrical, Electronic, and Information Engineering, Università di Bologna, 40123 Bologna, Italy

Color versions of one or more of the figures in this paper are available online at http://ieeexplore.ieee.org.

Digital Object Identifier 10.1109/TIM.2018.2890187

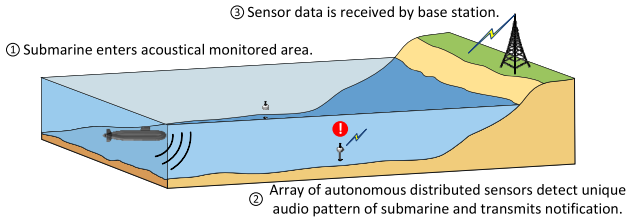

Fig. 1. High-level overview of the underwater detection scenario.

Underwater acoustic monitoring has been a topic of active research with great impact and interest in the study of marine life, pollution monitoring, unmanned autonomous vehicles, oil extraction, and monitoring, aquaculture monitoring and tactical surveillance [4]–[7]. Underwater acoustic sensor networks are wireless sensor networks especially designed for aqueous environments for underwater applications, whose implementations and operations are solely based on acoustic measurements and communications [5]. Recognizing environmental sounds is a signal-processing problem that requires sound acquisition, conversion, and processing. These tasks require continuous operation and consume power even when there is no useful information to process [8]–[10].

Duty cycling is an effective way to reduce power consumption and thereby improve the lifetime of sensors supplied by batteries in commercially available and academic solutions [11]. An alternative and promising approach is to design low-power event-driven sensors to detect events of interest continuously, keeping the power consumption very low, at least an order of magnitude lower than the sensor itself in active mode [12]–[17]. Event-driven sensors are a step toward self-sustainable sensing paradigm when environmental energy is used to power the low-power sensor and replenish its energy storage [18]. Self-sustainability enables always-on perpetual monitoring and detection of important events. To achieve this ambitious goal, sensors need on the one hand to reduce the power consumption and increase the capabilities to detect events; on the other hand, they must embed a subsystem to extract the energy from the monitored environment, such as novel microbial fuel cells (MFCs) [19]–[27].

Fig. 1 shows a high-level overview of an underwater application scenario, where several autonomous sensors are placed under the water to detect events of interest (i.e., a submarine or other vehicles), and as soon as the event is detected, a wireless message is sent. Although the designed acoustic detector can be used in several applications, in this

paper, we focus on long-term underwater monitoring. This paper extends the work presented in [28].

The main contributions of this paper and the improvements with respect to earlier work in [28] are as follows.

1) The always-on event-driven audio detector has been redesigned incorporating an active envelope detector, which improves the overall sensitivity to more than 20 dB using only 7-μW additional power. Measurements have experimentally verified the performance of this new detector.
2) The microbial fuel cell and the energy harvesting circuits have been optimized and characterized by extensive experimental results.
3) A stand-alone version of the self-sustaining event-driven detector has been implemented to perform accurate experimental measurements to evaluate the performance and to demonstrate perpetual work with four commercial MFCs connected in a series–parallel configuration.

II. Related Works

Recent literature has examples for video/image, audio, inertial, and other sensors that are showing promising results regarding energy efficiency and power saving [14]–[19]. In particular, event-driven approaches allow reducing the power consumption to acquire and process environment data when there are no relevant data to be detected [27]. There is also an example of a commercially available audio trigger that shows the relevance of this new promising approach [29]. Delbruck *et al.* [30] designed a fully integrated wake-up circuit within a power-budget of 500 μW for acoustic detectors, which recognizes human speech. In [9], a basic concept of event-driven acoustic detector that performs temporal-frequency audio features with discrete components is presented. This solution consumes only 13.5 μW. However, this detector is tuned for a single frequency channel, and the pattern detection is not presented, but just mentioned. There are also customized integrated chip solutions for audio applications. A very low-power multifrequency solution is presented in [31], where Katsiamis *et al.* designed a spectral decomposition circuit using an analog bandpass filter. The solution from Katsiamis *et al.* [31] achieved only 4.5 μW of power consumption. However, the digital processing and the power of the microphone are not considered in this total. Another interesting solution is presented in [32], where a 16-channel analog filtering bank is presented. This solution consumes only 63.3 μW achieving high precision. Adaptive single-channel audio magnitude-detector has been implemented within a power budget of 1.1 μW in [32]; however, in a real application scenario, where multiple channels are required, multiple detectors need to be employed, increasing the overall power consumption. In [33], an analog bionic-ear (cochlea) CMOS chip has been presented with nine filter banks and overall power consumption of 60–90 μW. Finally, in [34] a novel micropower detector with multiple frequency bands is presented. The power consumption is only 6 μW in the active mode. However, the detector is tuned only for voice detection, and it needs an external microcontroller to perform programmable data analysis.

Unlike the previous works, our work is a standalone ultralow power single-channel solution, which is programmable and more flexible with up to eight run-time tunable frequencies. Thanks to low power design and feature extraction in the analog front-end, our solution has a similar power consumption to other integrated state-of-the-art solutions. Due to the presence of a microcontroller on board, we provide a programmable detector that can be trained for different audio patterns and application scenarios. As we have shown, even recent analog integrated circuits have a similar power consumption to our solution; however, they are not achieving better performance and functionality, and they have very limited programmability. Moreover, in many applications, discrete components speeds-up the development time and reduces the cost of the solution.

Although low power consumption and event-driven sensors are important to keep the power as low as possible, they are not sufficient to guarantee perpetual monitoring. Energy harvesting from environmental sources is a key technology to achieve a self-sustaining smart sensor [20]–[25]. Combining energy harvesting and low-power design could result to have self-sustainable always-on sensing. Trigona *et al.* [35] proposed a novel approach named "zero-current standby" to achieve a self-sustaining current sensor. The system can acquire energy from the movements, for instance when deployed on the human body, and give information on the motion as well. Prieto *et al.* [36] proposed a multisource energy harvesting acoustic system for indoor monitoring. The available energy harvesting input is photovoltaic, thermal, and vibration. The design of the processing is based on a microcontroller, which consumes significantly more power than our solution. Nevertheless, the authors demonstrate that it is possible to achieve a self-sustaining operation that confirms the benefits of coupling energy harvesting with smart sensing.

A promising novel technology to improve the energy availability of underwater sensors is using sediment MFCs that can generate μW of power continuously and without the need for replacement or maintenance [19], [24]. Recent literature demonstrates that MFCs are a valid alternative renewable power source for smart sensors that are not only limited to underwater deployments [5], [23], [24]. Combination of low power consumption, intelligent event-driven detector, energy harvesting, and aggressive power management has emerged as one of the most promising techniques to achieve self-sustaining smart sensing for internet of things and underwater monitoring [26]. This paper extends the work proposed in [28] providing an improved design of the detector and more solid and accurate experimental results. Except for this previous work, there is no self-sustaining underwater acoustic monitoring solution available as a research prototype or commercial product. Moreover, in this paper, we optimize the conversion subsystem and the use of the available energy to achieve a smart sensor that works perpetually. We implemented and evaluated a working prototype to be deployed underwater.

III. Background

The most popular approach to process acoustic data to extract useful information or a specific pattern is extracting the spectral information of the audio signal in time [37].

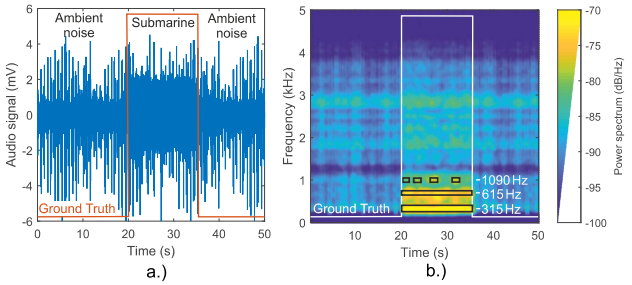

Fig. 2. Audio signal of a submarine superimposed with ambient noise (a) in the time domain, (b) spectral–temporal representation of the same signal where the specific audio pattern is highlighted in black identifying activity in three frequency bands centered around 315, 615, and 1090 Hz.

For example, state-of-the-art machine learning classifiers use time–frequency representations of the audio signals to detect and classify events [28], [10], [37]. Machine learning is used to find and tag events that occur in an unconstrained environmental audio stream automatically [37].

Fig. 2 shows an acoustic signal featuring a submarine engine and ambient noise in the time domain (a) and the time-frequency representation of the same signals (b). The specific time–frequency audio pattern is highlighted between time = 20 s and time = 35 s, in particular in (b), with three black rectangles identifying activity in three frequency bands with a dominant power spectrum below of −75 dB/Hz. The lower two bands, at 315 and 615 Hz, represent the submarine engine sound, whereas the cavitation effect causes the discontinuous 1090-Hz band. Cavitation and the corresponding noise originate from collapsing air bubbles at higher propeller speeds as a function of water pressure. Due to those features, which are not present in the ambient noise, machine-learning algorithms can be trained to classify or to detect the specific audio pattern.

Smart audio sensors continuously looking for audio events are required to acquire data from microphones, convert the analog time output signal [Fig. 2(a)] to a digital form with an analog-to-digital converter and subsequently process the data extracting the frequency features to classify the sound. These tasks are typically performed by ultralow-power systems using at least a few mW of power that can drain a typical Li-Ion battery in a few hours. A traditional approach to reducing the overall power consumption is the polling approach (or duty cycling). The upper part of Fig. 3 shows the polling approach where the system is off for a predetermined period (T_{off}) to save energy and activated for a small portion of time (T_{on}). There is a tradeoff between the power saved (longer T_{off}) and the probability not to miss an event (short T_{off}). A novel approach, adopted in this paper, to save power without losing any event is shown at the bottom half of Fig. 3, where the system uses an always-on event-driven detector to catch the event of interest and wakes up the rest of circuit once a probable event is detected. One of the most important features of the always-on circuitry is to consume an order of magnitude lower power than the sensing system in active mode. Designing such a low-power audio detector, which is based on an event-driven approach, with a power budget of less than 100 μW is the main goal of this paper.

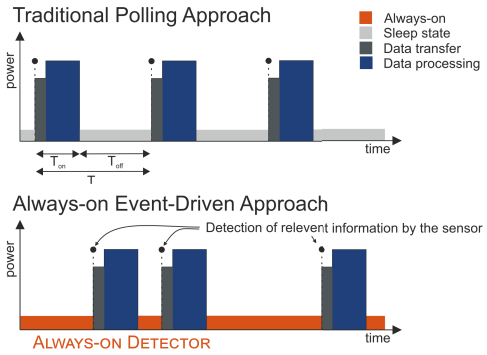

Fig. 3. Traditional polling approach where the system is off for a predetermined period (T_{off}) to save energy and activated for a small portion of time T_{on} versus always-on even-driven approach where an ultralow-power detector is continuously processing the information to detect relevant events before waking up the rest of the system.

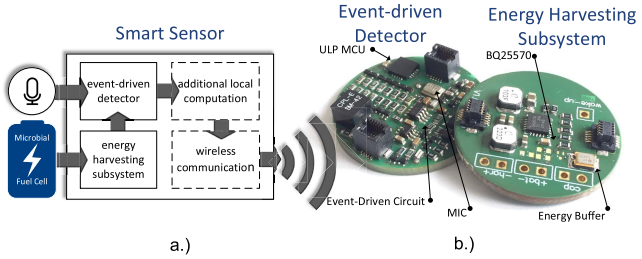

Fig. 4. Underwater wireless sensor node supplied by the microbial fuel cell, including the event-driven audio detector (right). A prototype of the always-on audio detector that includes the event-driven audio detector and the microbial fuel cell subsystem to constantly supply the detector and recharge the energy buffer (left).

The proposed design exploits the relatively slow rate of change (in the range of milliseconds) of the audio signals of interest, which are engine and propeller noise, to serialize the frequency features extraction with an adaptable mixed-signal circuit. Section IV presents details of the proposed design.

IV. System Architecture

Fig. 4 illustrates the block diagram of a smart wireless sensor exploiting MFCs to achieve self-sustainability. In this paper, we present a programmable event-driven audio detector comprised by an analog front-end with the feature-extraction capability and an ultralow-power microcontroller for pattern recognition. An energy harvesting subsystem, optimized for small-size MFCs, allows the full system to be self-sustaining.

The section is divided into two subsections. Section IV-A presents the hardware architecture of the proposed always-on event-driven audio detector. Section IV-B presents the algorithm implemented in the ultralow-power microcontroller to achieve time–frequency pattern detection. Section V will describe the energy harvesting subsystem designed to host MFCs.

A. Event-Driven Audio Detector: Hardware Architecture

Fig. 5 shows the hardware architecture of the novel low-power event-driven detector that can work with any commercial analog sensor. In this implementation, the microphone

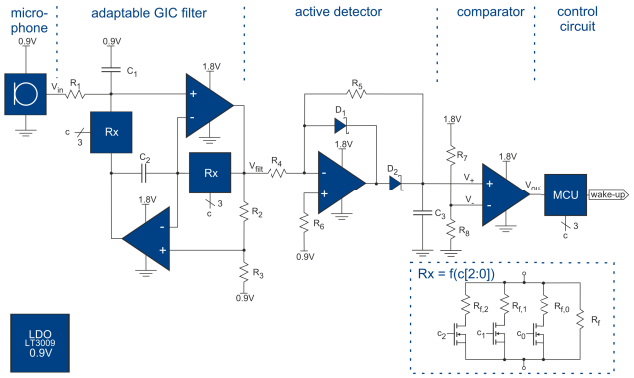

Fig. 5. Architecture of the designed ultralow-power event-driven audio detector

selected is a low-power and low-noise commercial MEMS analog microphone from InvenSense (ICS-40310) that consumes only 16 μA at 0.9 V in always-on mode. The main goal of the designed detector is to extract time-frequency features from the analog input with an analog ultra-low power and tunable front-end. To achieve this goal, we designed an adaptable generalized impedance converter (GIC) and a time detector comprised by an active envelope detector and a comparator. The circuit is designed using OPA379 ultralow-power operational amplifiers from Texas Instruments consuming only 2.9 μA at 1.8 V with a gain bandwidth product of 90 KHz. Due to these features, it is possible to design a GIC filter, which detects frequencies between 10 Hz and 10 kHz changing the variable resistance blocks according to the following equation:

$$f_c = \frac{1}{2\pi\, Rx C} \tag{1}$$

where f_c is the selected corner frequency of the detector, R the variable resistance that is tuned by the bits c[2:0] of the microcontroller, and $C = C_1 = C_2$. The adaptable resistance $R(c_x)$ is realized with a passive discrete parallel structure of resistors and n-channel metal–oxide–semiconductor-field-effect transistors (MOSFET) as shown in Fig. 5 (bottom inset). The resistance can be calculated using the following equation:

$$Rx = R(c[2:0]) = \frac{1}{\frac{1}{R_f} + \sum_{i=0}^{2} \frac{c_i}{R_{f,i}}}. \tag{2}$$

In this version, we connect three general-purpose input–output (GPIO) pins of the microcontroller to the gates of the MOSFETs to tune the variable resistance with eight (2^3) different values, that result in eight tunable frequencies. Transistors with low drain–source capacitance are employed to guarantee stable operation reducing the effect of the parasitic capacitance in the feedback path. The variable resistance block has been tuned to have frequencies from 300 to 3700 Hz. The transfer characteristic of the adaptable bandpass filter is analyzed in the experimental section. The frequency switch takes an average of 100 ms to allow the GIC and the detector to have a stable output for the lower frequency.

After the adaptive GIC that extracts the frequency features of interest, the temporal features are generated enveloping the filter output with an active peak detector. The detector amplifies the bandpass filtered signal by the ratio of the resistor R_4 and R_5 according to the following equation:

$$G = -\frac{R_5}{R_4}. \tag{3}$$

Due to the use of the active peak detector, it is possible to achieve higher sensitivity compared with a solution with passive diodes [28].

In the next stage, an ultralow-power comparator, LPV7215 from Texas Instruments, which consumes 580 nA at 1.8 V is used to compare the signal with a defined reference. Thus, the output of the comparator V_{out} will be "high" for the duration of the detected frequency of the GIC and "low" otherwise. By checking V_{out}, an ultralow-power microcontroller can detect when a specific frequency is present and how long it lasts.

When multiple frequencies are simultaneously present in the audio pattern of interest, the microcontroller can dynamically change the frequencies of the adaptive GIC according to the trained audio pattern. As the main goal of this design is low power consumption and intelligence on board, the selected microcontroller (MCU) is the PIC16LF1509 from Microchip configured to work with the internal 31 kHz oscillator consuming only 4.3 μW in active mode.

In underwater applications, the MEMS microphone can be replaced with an analog hydrophone.

B. Event-Driven Audio Detector: Microcontroller Algorithm

While the first goal of the design is to minimize the power consumption of the analog front-end, the second goal is to achieve a programmable detector, which can be trained to recognize different audio patterns. Thus, the audio detector includes an ultralow-power microcontroller which processes the spectral-temporal features of the analog front-end presented in the previous subsection and can be trained to recognize specific patterns. Fig. 7 shows the flowchart of the implemented algorithm, which can be separated into three parts: 1) idle; 2) repeated acquisition; and 3) classification.

1) Idle: To reduce the overall power consumption, the MCU is in sleep mode as much as possible. Thus, in the *idle*, the audio detector is configured to monitor continuously only a single spectral component. When the first frequency of interest, 315 Hz in our example, is detected, a trigger is generated by the analog circuit, and the microcontroller wakes up and goes into *repeated acquisition* mode.

2) Repeated Acquisition: The corner frequency of the filter is iteratively adapted, a 100-ms timer is started to ensure that the output of the event-driven circuit is settled. Following the timer overflow, the output signal of the comparator is stored, and the GIC filter is adapted to the next higher corner frequency. This procedure is repeated for each possible filter setting.

3) Classification: The measured spectral components are compared with the trained pattern-specific spectral components. To save memory, we combine the output of all eight channels in one byte where each bit shows the "1," or absence "0," of the spectral components in the 100-ms time window. Fig. 6 shows an example pattern specific vector (in this case, the submarine noise) which includes three

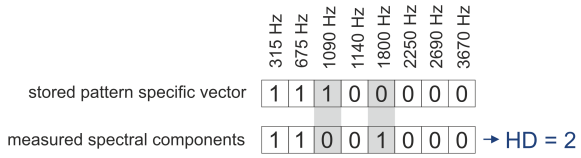

Fig. 6. Classification of the measured spectral components by comparing them to the stored pattern specific vector.

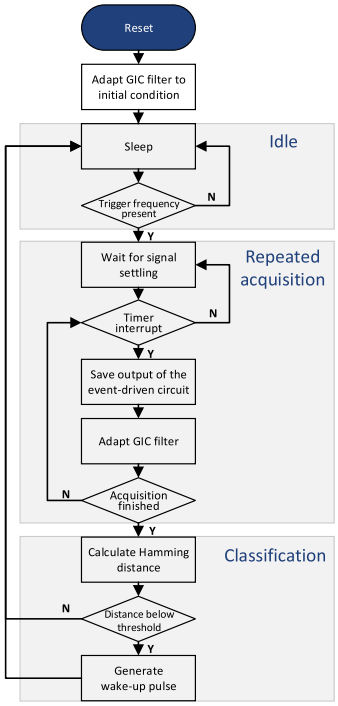

Fig. 7. Algorithm implemented in the ultralow-power MCU to detect specific patterns.

dominant frequencies that need to be present and other five frequencies that need to be absent in the audio. The Hamming distance between the measured binary vector, consisting out of the eight analyzed spectral components and the corresponding vector that stored pattern specific components is then calculated. When the hamming distance is below a selectable threshold, the audio detector generates a signal.

The algorithm can be tuned with three possible thresholds: 0 (HD0), 1 (HD1), 2 (HD2), which represent the maximum number of bits that are different between the two vectors. For example, in Fig. 6, we have a Hamming difference of two. The thresholds affect the accuracy of the algorithm as we evaluate in the experimental results section. After every classification, the MCU sets the circuit back to the initial state detecting the first frequency, and it goes into sleep mode until the next first frequency of interest is detected.

V. Microbial Fuel Cell Energy Harvesting

MFCs that use sediment and natural metabolisms of microbes have shown to be an effective energy source for underwater applications [24]–[26], [39]. The most common two-chamber MFC configuration consists of two compartments separated by an ion exchange membrane. The anode

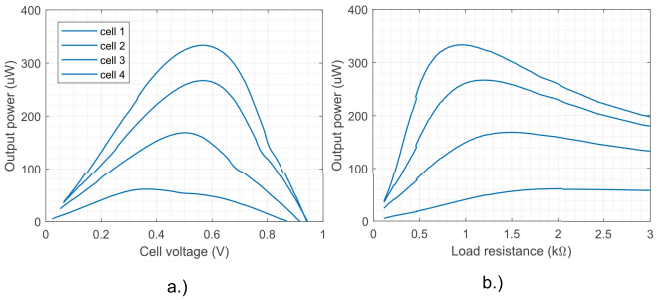

Fig. 8. Output power versus (a) open circuit voltage and (b) load resistance of four different MFCs in the same condition, during the load sweep.

containing half-cell is filled with fuel (anolyte) and specific microbes, which catalyze the anode reaction [23]. These microorganisms have to be added, or they are already present such as in the wastewater or sea underwater. The second compartment contains the cathode as well as the MFC oxidant (catholyte). The microbes that build a biofilm on the surface of the anode benefit from the process by extracting small amounts of the potential energy of passing electrons to fulfill their energy demand. In addition, they use the fuel as a carbon source [23]. Previous recent works [24] and [39] evaluated the capability, the power, and the voltages of the sea-sediments microbial fuel cell. As the main goal of this paper is to design a system able to harvest energy from MFC, we characterized MudWatt technology kits (Keego Technologies, LLC, Menlo Park, CA, USA) as a reference input [40]. MudWatt is a commercial kit designed to generate energy from microbes from soil, sea sediments, and water waste [40]. MudWatt exploits microbes to generate energy using a graphite fiber felt anode (thickness 0.5 cm, diameter 8 cm) and cathode (thickness 1 cm diameter 8.5 cm) and titanium wires. As a first step we performed a thorough characterization of the MFC system to match our circuit so that it can work with a suitable configuration of MFCs in terms of voltage, power, and current needed support self-sustaining operation. For the evaluation, multiple cells are placed in the same conditions of uniform initial humidity and soil. The experiments have been performed at a controlled temperature of +5 °C. The electrical potential of the cells is monitored during the growing phase of the microbes. Afterward, open circuit voltage is measured, as well as the cell behavior during different load situations. Fig. 8 shows the measured output power. On the left chart, the output power plots are presented according to the open circuit voltage; on the right chart, the output power is plotted as a function of the load resistance. Experiments show significant variability in MFCs cell performance, even when cells are in the same initial conditions. This difference is mainly due to the fact MFCs comprised by living microbes growing differently in different MFCs. In addition, power generation within MFC is a complex process that is affected by soil homogeneity, moisture, available nutrition, biofilm thickness, to mention a few dominant variables. From our measurements, we reported a worst case cell that has an open circuit voltage of around 0.8 V and a peak output power in the range of 50 μW. The maximal power point is obtained by fixing the voltage between the 50% and 60% of the open circuit voltage.

The best cells show up to six times higher peak output power of 330 μW than other healthy cells. Load resistance varies between 800 Ω and 2 kΩ at the maximal power point (MPP). For the measurements, a settling time of seconds, close to the open circuit voltage of several minutes, has to be considered between single data points. Without sufficient time to adapt to a new load situation, the cell will shortly provide more power compared to a constant load situation.

A. Energy Harvesting Subsystem

A critical role of the energy harvesting subsystem is to convert and transfer energy from a specific source to energy storage, maximizing the energy conversion. The conversion efficiency is the most important parameter to avoid wasting precious energy in the conversion. As we presented in the previous subsection, MFCs are not a stable power source, so it is even more important to keep the MFCs in the maximum power point in all the operating conditions to maximize the power extracted. To achieve this goal, we designed an energy harvesting subsystem around the state-of-the-art integrated circuit from Texas Instruments, BQ25570. This choice is due to the presence of a high-efficiency boost converter, which can harvest energy from sub-milliwatt low-voltage sources down to 100 mV. Moreover, the BQ25570 features a programmable maximum power point tracking (MPPT) capabilities to achieve up to 90% of conversion efficiency. Thus, the converter input impedance is periodically adapted by regulating the harvester input voltage. MPPT allows the harvester to match to changes in the MFC output power and maximize the energy conversion. Finally, it integrates an ultralow-power buck converter that was tuned in our design to 1.8 V to supply the entire system shown in Fig. 5. The harvesting subsystem consumes only 488 nA while it is harvesting energy and is supplying the system. Although the BQ25570 is optimized for low-power energy sources, and it achieves a maximum efficiency of up to 90%, this conversion efficiency is highly dependent on the input voltage, input power, and the voltage of the storage. In fact, from our measurements and the datasheet of BQ25570, this 90% efficiency is achieved only for input voltage levels above 1.4 V and current above 100 μA. For this reason, multiple MFCs need to be used to reduce conversion losses. In our experimental evaluation, we used four MFCs in series–parallel configurations (two in series and two in parallel).

VI. Experimental Results

Fig. 4 (on the right) shows the designed prototype that incorporates both the MFC energy harvesting subsystem and the event-driven audio detector on two stackable circuit boards (PCBs). The prototype has been designed and developed to test functionality, power consumption, and efficiency of the energy harvesting subsystem as well as for audio detector characterization regarding detection performance and sensitivity. Moreover, we designed a stand-alone system including the event-driven audio detector to experimentally evaluate the feasibility to achieve a self-sustaining smart audio detector that works perpetually with MFCs as an energy source. In this current implementation, the audio detector has been tuned to recognize a submarine motor noise and generate a trigger when the sound is detected.

TABLE I
Power Consumption of the Always-On Audio Detector

Consumption measured @1.8V		
Subsystems/Tasks	***Current (μA)***	***Power (μW)***
LDO 0.9V	4.22	7.60
Microphone [a]	15.76	28.37
Time-Frequency detector	12.55	22.59
MCU - Processing	2.39	4.30
MCU - Idle	0.02	0.04
Detection of multiple freq.	**34.92**	**62.86**
Idle (Waiting for the first freq)	**32.75**	**58.95**

[a] Measurement of the microphone and the 0.9V circuits includes conversion loss from 1.8V to 0.9V

A. Power Consumption With Experimental Measurements

Table I shows the power consumption of different subsystems/tasks of the prototype. We measured the power consumption of the whole detector in the idle-state, waiting for a single frequency when the ULP MCU is in sleep mode, and during multiple time–frequency detections when the ULP MCU is in active mode looking for the specific pattern, as presented in Section V. It can be noticed that the microphone is the most power-hungry component in our solution consuming alone around 35 μW including the conversion power lost due to the voltage regulator to convert 1.8 V of the energy harvesting subsystem to 0.9 V needed to supply the microphone. Thus, our low power time—frequency detector consumes only 22.59 μW, while the ULP MCU clocked at 31 kHz consumes around 4 μW in active mode and only 36 nW in sleep mode. As it can be seen, during the pattern detection when the MCU is in active mode, and the time-frequency circuits are periodically updated, the whole detector consumes only 63 μW. However, our designed time–frequency programmable detector, front-end plus MCU, consumes only 26.89 μW in the worst case of processing data, which confirms the low-power design of the event-driven circuits.

B. Measurement Setup

For automated measurements with a high sample rate, the National Instruments USB-6216 DAQ system has been employed. Fig. 9 shows the typical measurement setup. The energy harvesting subsystem has been connected on an expansion board for easy access to electrical signals of interest. As power source four MFCs, described in Section V, in two series and two parallel configurations have been used. After the characterization to accurately repeat the measurements in defined conditions, a Keysight B2912A precision source/measure unit is used as input of the energy harvesting circuit to emulate the MFCs. Measuring instruments, as well as circuit configuration, are controlled via MATLAB. To adapt the always-on audio detector during characterization a test firmware that allows configuration of the circuit via GPIOs controlled by the DAQ system is used.

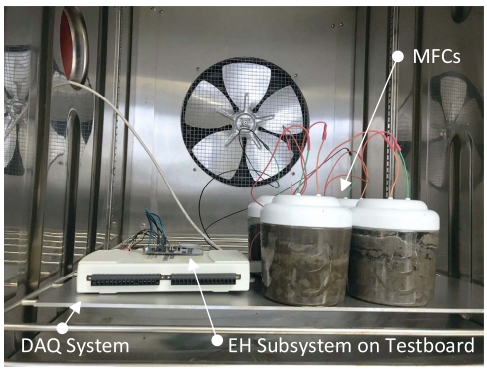

Fig. 9. Typical used measurement setup for the characterization of the subsystems. The MFCs from Keego Technologies are shown in the lower right corner.

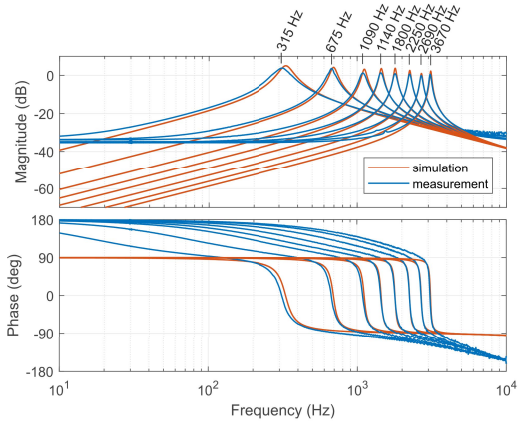

Fig. 10. Bode diagram of the adaptable GIC bandpass filter simulated with SPICE and measured in the real implementation.

C. Adaptable Filter Transfer Function

The transfer function of the adaptable 3-bit GIC bandpass filter is shown in Fig. 10 both with SPICE simulations (red) and actual measured filter characteristics For the measurements, a sine-shaped signal with 200-mV amplitude and 0.5-V dc component is generated by the DAQ system as a stand-in for the microphone. Input signal as well as the filter output V_{filt} is measured for 100 periods at every data point. Subsequently the phase information with cross correlation and the magnitude is calculated. The deviation from the design parameter of the corner frequencies is mainly caused by the discrete component values as well as their tolerances. The corner frequencies of the filter are chosen according to the frequency pattern of interest in our application.

D. Circuit Sensitivity

To measure the worst case sensitivity of the analog input section in a controlled environment, the microphone is replaced with a function generator and the adaptable filter is configured to a corner frequency of 1 kHz. The amplitude of ON–OFF keying modulated 1-kHz sine-shaped signal is reduced until the comparator output signal V_{out} stops to follow input modulation. From the smallest detectable signal peak-to-peak amplitude of 1.25 mV, the voltage sensitivity

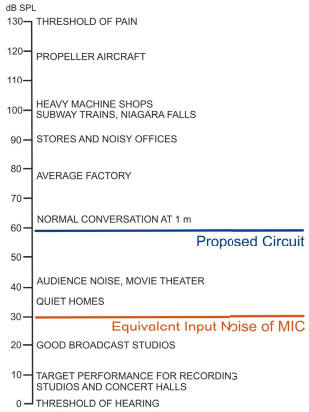

Fig. 11. Sensitivity of the always-on acoustic detector in perspective [42].

can be calculated according to the following equation to −67.12 dB(V)

$$\text{Sensitivity}_{\text{dB(V)@1 kHz}} = 20\log\left(\frac{V_{pp,\min}\frac{1}{2\sqrt{2}}}{1\ \text{V}}\right). \quad (4)$$

Considering the −37 dB (V) sensitivity of the used ICS-40310 microphone from InvenSense [41], the theoretical minimal acoustical sensitivity follows equation to 63.88-dB sound pressure level (SPL)

$$\text{Sensitivity}_{\text{dB(SPL)}} = \text{Reference}_{\text{SPL}} + (\text{Sensitivity}_{\text{dB(V)@1 kHz}} - \text{Sensitivity}_{\text{mic}}). \quad (5)$$

When the designed system, including the microphone and the recognition algorithm, has been characterized, the sensitivity has been measured as 59 dB (SPL), respectively, 0.71 mV_{pp}. The increased sensitivity compared to the worst case scenario is due to an observation time of several seconds in the target application. During the measurements, the ambient noise was in average 55 dB (SPL), and the SPL was measured close to the microphone with a sound level meter. Fig. 11 shows the sensitivity of the low power detection circuit is in the range of a typical conversation at 1-m distance. In underwater monitoring and with the noise of the marine motor this will be sufficient to detect submarine engines to several meters of distance.

E. Pattern Detection

The corner frequencies of the input filter are selected according to the dominant spectral components in submarine noise recorded with hydrophones and provided by the San Francisco Maritime National Park Association [43]. To train the detection algorithm the spectral information of the audio files is analyzed offline to identify the spectral-temporal feature for the signal of interest. This allows extracting the pattern specific binary vector, which is used by the microcontroller algorithm to classify the audio stream as described in Section IV-B. After the training three dominant frequencies at 315, 675, and 1090 Hz have been selected and the detector has been programed to detect submarine noise exploiting these three frequencies.

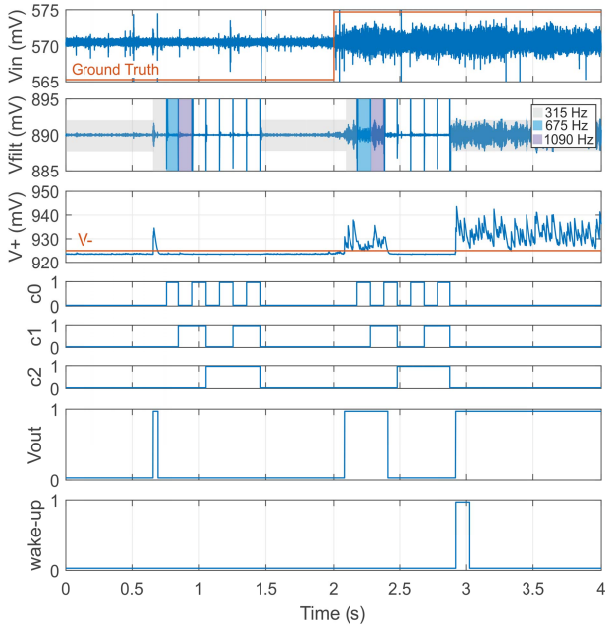

Fig. 12. Circuit response and pattern detection generated by the ultralow-power microcontroller when evaluating a test audio sequence. The submarine engine noise starts at 2 s.

Fig. 12 shows the circuit response during the detection and the classification of a submarine noise recorded with a hydrophone and played in our laboratory. After 2 s, the submarine engine noise starts. The first subplot (top) of Fig. 12 shows the analog output of the microphone (V_{in}), which is the input for the event-driven detector. The second subplot visualizes the bandpass filter output (V_{filt}) and its corner frequency adaption during the detection sequence. The third subplot shows the positive comparator input signal V_+ and the constant negative threshold V_-. The following five subplots display the control lines for the adaption of the GIC filter (c_0, c_1, c_2), the comparator output V_{out}, which is connected to the ULP MCU, and the wake-up signal generated by the detector.

At the starting time 0 s, the filter is tuned to 315 Hz highlighted light gray. After approximately $t = 0.65$ s the input signal contains the frequency component with an amplitude V_+ that exceeds the negative threshold, and the comparator triggers the microcontroller for a classification sequence. During the classification sequence, the filter is adapted with the control lines c_0, c_1, and c_2 in a linear manner from the lowest to the highest corner frequency and the comparator response is stored. At the time $t = 1.45$ s, the MCU compares the measured frequency components with the pattern specific stored data. Due to the lack of the 675- and 1090-Hz components, no wake-up pulse is generated, and the circuit goes into sleep state again. At $t = 2.1$ s, a second detection sequence is triggered by a 315-Hz component in the input signal. This time, all three dominant frequencies of the submarine audio pattern are present and detected, as it is evident by the threshold exceeding V_+ and high V_{out} signal between 2.1 and 2.4 s. Subsequent, between $t = 2.4$ s and $t = 2.9$ s, the absent frequency components between 1140 and 3670 Hz are analyzed.

TABLE II
DETECTION PERFORMANCE

	Sub marine	*Ambient noise*	*Ship*	*Heavy rain*	*Light rain*	*Surface ice*	*ACC*
HD0	**40.67% (TP)**	100% (TN)	99.33% (TN)	100% (TN)	100% (TN)	100% (TN)	**23.52%**
	57.33% (FN)	0% (FP)	0.67% (FP)	0% (FP)	0% (FP)	0% (FP)	
HD1	**98.67%**	100%	86%	94%	98%	98.67%	**95.89%**
	1.33%	0%	14%	6%	2%	1.33%	
HD2	**100%**	35.33%	0.67%	16.67%	70%	45.33%	**44.72%**
	0%	64.66%	99.33%	83.33%	30%	54.67%	

After the full sequence, the MCU generates an interrupt by activating a GPIO output when the audio pattern is detected ($t = 2.9$ s), visible in the last subplot. From time $t = 3$ s to $t = 4$ s the submarine noise is still present as well as the 315-Hz frequency component. As a result, the positive comparator input voltage V_+ exceeds the threshold and V_{out} stays high. A rising V_{out} signal would trigger the next classification sequence. To evaluate the accuracy of the detection with experimental measurements, we played different audio streams (Ambient noise, Submarines motor, Ship motor, Heavy rain, Light rain, Surface ice) recorded with a hydrophone using the data set provided by San Francisco Maritime National Park Association [43]. Every audio stream lasts 20 s and we ran experiments totaling 5 h of audio playbacks. During the experiments, 150 samples of each sound have been played in a random sequence. The average microphone output voltage was 0.8 mV_{pp} and thus 60 dB(SPL) in the proximity of the detector. As we mentioned the event-driven detector has been configured to detect only the submarine noise [true positive (TP)], and it does not generate wake-up pulses for the others [true negative (TN)]. In our evaluation, a false negative (FN) is counted when wake-up pulses do not occur despite the presence of the submarine pattern. For all the other audio streams (Ambient Noise, Ship, Heavy Rain, Light Rain, Surface ice) we consider a false positive (FP) when the detector generates a wake-up pulse in the presence of these sounds.

Table II shows the circuit response for different Hamming Distances: 0 (HD0); 1 (HD1); 2 (HD2). As described in Section IV-B, the Hamming distance is calculated between the stored pattern specific vector and the measured frequency components before a possible wake-up pulse occurs. The minimal allowed Hamming distance for generating a wake-up pulse can be used to adapt the circuit to subsequent higher power higher precision detectors.

Table II shows a very low percentage of TP in HD0 conditions that means the Hamming distance 0 is not optimal to recognize the submarine noise. With a hamming distance of 2 (HD2), the submarine pattern has always been recognized correctly. However, in HD2, the number of FP due to other sounds is very high, up to 99.33% for the ship noise. Finally, HD1 provides high performance in TP (up to 98.67%) with a low level of FP (worst case 14% for the ship sounds). The overall accuracy (ACC) is evaluated taking TP, FN, TN, and

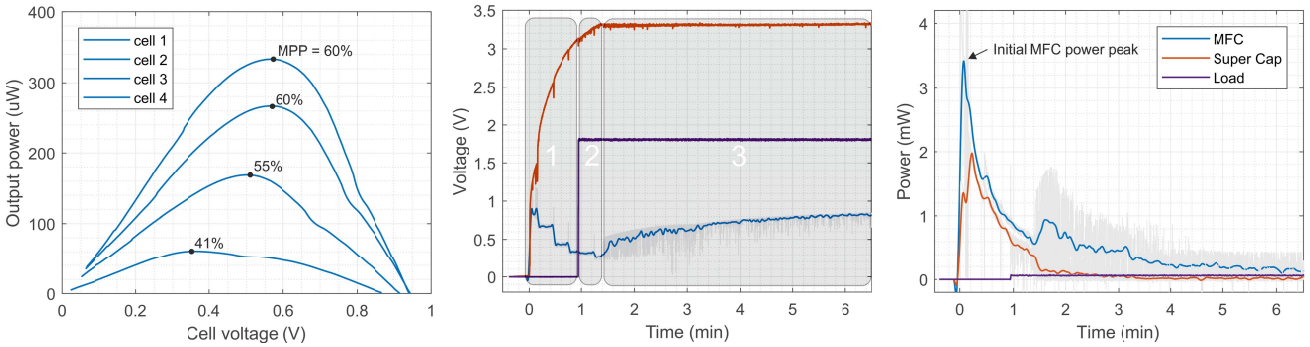

Fig. 13. Cold start and perpetual work phase of the event-driven detector working with MFCs. The experiments show that the developed prototype achieves a self-sustainable smart sensing combining the low-power always-on event-driven detector and MFC that even generates a surplus on energy that can be used by other circuits (i.e., sending a message or performing more power-hungry processing) that we are not considering in this paper.

FP according to the following equation:

$$\mathrm{ACC} = \frac{\mathrm{TP} + \mathrm{TN}}{\mathrm{TP} + \mathrm{TN} + \mathrm{FN} + \mathrm{FP}}. \tag{6}$$

Applying (6) for different Hamming distances, then to the three different rows in Table II, the maximal achieved accuracy is 95.89%, which can be obtained with HD1 as expected.

F. Self-Sustaining Always-On Sensing With MFC

Fig. 13(b) and (c) shows the behavior of the whole system. The energy-harvesting block consists of four MFCs in two serial, two parallel combinations and the energy harvesting subsystem. To demonstrate the capability to deploy the system under the sea we connected a completely discharged supercapacitor of 11 mF as an energy buffer to evaluate the realistic and challenging cold-start phase of the harvesting system. The capacitance is matched to the MFC behavior, which allows buffering as much energy as possible with the parallel support of the cold start. The MPP tracking is programmed to 50%, the maximal supercapacitor voltage is 3.3 V, and the load of the system is the audio detector with 60 μW of power consumption.

At $t = 0$ the four MFC cells are connected to the circuit. The MFCs completely charge the supercapacitor in the first 80 s, harvesting significantly more energy than they would supply the smart detector. This surplus is used to overcome the harvesting circuit cold-start phase and allow full operation of the circuit in less than one minute.

Fig 13(b) shows the voltages of the cells, the battery, and the load in three typical phases: 1) the cold-start phase, which ends with switching on the 1.8 V supply of the subsequent detection circuit. The threshold is hardware programmable and depends on the battery voltage. 2) In the second phase, the detector is fully working, and the capacitor is charged until the maximal programmed voltage. During the first two phases, the harvesting circuit periodically adapts the load which can be seen by the cascade shaped MFC voltage. This is required due to dropping cell voltages and controlled by the MPPT algorithm of the harvesting circuit. 3) In the final phase, perpetual work, the supercapacitor is fully charged.

In this operation mode, the harvesting circuit significantly reduces the load with parallel higher switching frequency, visualized in light gray. The reduced load allows the cell voltages to recover until an equilibrium is reached slowly.

VII. Conclusion

In this paper, we have developed and experimentally verified perpetual operation of a smart acoustic sensing node for underwater deployment. This operation is made possible by two key contributions: 1) designing an adaptive ultralow power event-driven audio detector with eight run-time tunable frequencies, that allows the majority of the system to remain in a low power idle mode using just (60 μW) and 2) by adopting an energy harvesting scheme based on MFCs to be used in this application domain. A whole system has been developed, and it can be trained to recognize audio patterns and to generate triggers with an accuracy up to 95.89%. Accurate measurements have been presented, which show the detector consumes only 26.89 μW in always-on mode, achieving a sensitivity of 59 dB (SPL). The whole system including the microphone consumes only 62 μW, and it can be perpetually supplied by small size MFCs to achieve a self-sustaining underwater detector. The MFCs and the energy harvesting subsystem have been evaluated and presented in this paper. Future works will focus on real in-field evaluation in the underwater scenario, using small-size MFC [24] and deploying the smart sensors in the sea.

References

[1] J. Morgan. (2014). *A Simple Explanation of 'the Internet of Things.'* Accessed: Nov. 20, 2015.

[2] M. Bassoli, V. Bianchi, I. De Munari, and P. Ciampolini, "An IoT approach for an AAL Wi-Fi-based monitoring system," *IEEE Trans. Instrum. Meas.*, vol. 66, no. 12, pp. 3200–3209, Dec. 2017.

[3] *N-ZERO: A Zero Power Sensing Darpa Project*. Accessed: Oct. 10, 2018. [Online]. Available: https://www.darpa.mil/program/near-zero-rf-and-sensor-operations

[4] J. J. L. Aranda, S. Bader, and B. Oelmann, "An apparatus for the performance estimation of pressure fluctuation energy harvesters," *IEEE Trans. Instrum. Meas.*, vol. 67, no. 11, pp. 2705–2713, Nov. 2018.

[5] G. Han, C. Zhang, L. Shu, and J. J. P. C. Rodrigues, "Impacts of deployment strategies on localization performance in underwater acoustic sensor networks," *IEEE Trans. Ind. Electron.*, vol. 62, no. 3, pp. 1725–1733, Mar. 2015.

[6] V. M. Bhoopathy, M. B. H. Frej, S. R. E. Amalorpavaraj, and I. Shaik, "Localization and mobility of underwater acoustic sensor nodes," in *Proc. Annu. Connecticut Conf. Ind. Electron., Technol. Automat.* 2016, pp. 1–5.

[7] G. Xu, W. Shen, and X. Wang, "Applications of wireless sensor networks in marine environment monitoring: A survey," *Sensors*, vol. 14, no. 9, pp. 16932–16954, 2014.

[8] A. Thode, "An overview of research in underwater acoustics," *J. Acoust. Soc. Amer.*, vol. 139, no. 4, p. 2004, 2016.

[9] D. Oletic, V. Bilas, M. Magno, N. Felber, and L. Benini, "Low-power multichannel spectro-temporal feature extraction circuit for audio pattern wake-up," in *Proc. Design, Automat. Test Eur. Conf. Exhib. (DATE)*, 2016, pp. 355–360.

[10] S. Chu, S. Narayanan, and C.-C. J. Kuo, "Environmental sound recognition with time–frequency audio features," *IEEE Trans. Audio, Speech, Lang. Process.*, vol. 17, no. 6, pp. 1142–1158, Aug. 2009.

[11] B. Srbinovski, M. Magno, F. Edwards-Murphy, V. Pakrashi, and E. Popovici, "An energy aware adaptive sampling algorithm for energy harvesting WSN with energy hungry sensors," *Sensors*, vol. 16, no. 4, p. 448, 2016.

[12] R. H. Olsson, R. B. Bogoslovov, and C. Gordon, "Event driven persistent sensing: Overcoming the energy and lifetime limitations in unattended wireless sensors," in *Proc. IEEE SENSORS*, Oct./Nov. 2016, pp. 1–3.

[13] M. Magno, D. Brunelli, L. Thiele, and L. Benini, "Adaptive power control for solar harvesting multimodal wireless smart camera," in *Proc. 3rd ACM/IEEE Int. Conf. Distrib. Smart Cameras (ICDSC)*, Aug./Sep. 2009, pp. 1–7.

[14] S. Kim, G. Choi, S. Lee, J. Cho, and D. Park, "Event-detection microcontroller using interoperation-based acoustic surface sensing for individualized things-human interaction," *Int. J. Appl. Eng. Res.*, vol. 12, no. 12, pp. 3546–3552, 2017.

[15] Y. Hu *et al.*, "Event-driven wireless temperature sensor networks powered by air-flow based nanogenerator," in *Proc. IEEE 12th Int. Conf. Nano/Micro Eng. Mol. Syst. (NEMS)*, Apr. 2017, pp. 410–413.

[16] C. Kim, K. Bong, I. Hong, K. Lee, S. Choi, and H.-J. Yoo, "An ultra-low-power and mixed-mode event-driven face detection SoC for always-on mobile applications," in *Proc. ESSCIRC 43rd IEEE Eur. Solid State Circuits Conf.*, Sep. 2017, pp. 255–258.

[17] G. Singh, A. Nelson, S. Lu, R. Robucci, C. Patel, and N. Banerjee, "Event-driven low-power gesture recognition using differential capacitance," *IEEE Sensors J.*, vol. 16, no. 12, pp. 4955–4967, Jun. 2016.

[18] V. A. Aksyuk, "Internet of Things: Sensing without power," *Nature Nanotechnol.*, vol. 12, pp. 940–941, Sep. 2017.

[19] C. Santoro, F. Soavi, A. Serov, C. Arbizzani, and P. Atanassov, "Self-powered supercapacitive microbial fuel cell: The ultimate way of boosting and harvesting power," *Biosensors Bioelectron.*, vol. 78, pp. 229–235, Apr. 2016.

[20] M. Magno *et al.*, "InfiniTime: Multi-sensor wearable bracelet with human body harvesting," *Sustain. Comput., Inform. Syst.*, vol. 11, pp. 38–49, Sep. 2016.

[21] M. Thielen, L. Sigrist, M. Magno, C. Hierold, and L. Benini, "Human body heat for powering wearable devices: From thermal energy to application," *Energy Convers. Manage.*, vol. 131, pp. 44–54, Jan. 2017.

[22] M. T. Penella and M. Gasulla, "Runtime extension of low-power wireless sensor nodes using hybrid-storage units," *IEEE Trans. Instrum. Meas.*, vol. 59, no. 4, pp. 857–865, Apr. 2010.

[23] L. M. Tender, *Microbial Fuel Cells for Powering Navy Devices*. Washington, DC, USA: Naval Research Lab, 2014.

[24] Y. M. Arias-Thode *et al.*, "Demonstration of the SeptiStrand benthic microbial fuel cell powering a magnetometer for ship detection," *J. Power Sources*, vol. 356, pp. 419–429, Jul. 2017.

[25] G. Pasternak, J. Greenman, and I. Ieropoulos, "Self-powered, autonomous biological oxygen demand biosensor for online water quality monitoring," *Sens. Actuators B, Chem.*, vol. 244, pp. 815–822, Jun. 2017.

[26] C. E. Reimers and P. S. Schrader, and M. Wolf, "Autonomous sensors powered by a benthic microbial fuel cell provide long-term monitoring of the northeast pacific oxygen minimum zone," in *Proc. OCEANS Aberdeen*, Jun. 2017, pp. 1–4.

[27] A. Gomez, L. Sigrist, M. Magno, L. Benini, and L. Thiele, "Dynamic energy burst scaling for transiently powered systems," in *Proc. Conf. Design, Automat. Test Eur.*, 2016, pp. 349–354.

[28] P. Mayer, M. Magno, and L. Benini, "Combining microbial fuel cell and ultra-low power event-driven audio detector for zero-power sensing in underwater monitoring," in *Proc. IEEE Sensors Appl. Symp. (SAS)*, Seoul, South Korea, Mar. 2018, pp. 1–6.

[29] *Dolphin Integration: Low Power System on Chip*. Accessed: Oct. 10, 2018. [Online]. Available: https://www.dolphin-integration.com/

[30] T. Delbruck, T. Koch, R. Berner, and H. Hermansky, "Fully integrated 500 μw speech detection wake-up circuit," in *Proc. IEEE Int. Symp. Circuits Syst.*, May/Jun. 2010, pp. 2015–2018.

[31] A. G. Katsiamis, E. M. Drakakis, and R. F. Lyon, "A biomimetic, 4.5 μW, 120+db, log-domain cochlea channel with AGC," *IEEE J. Solid-State Circuits*, vol. 44, no. 3, pp. 1006–1022, Mar. 2009.

[32] B. Rumberg and D. W. Graham, "A low-power and high-precision programmable analog filter bank," *IEEE Trans. Circuits Syst. II, Exp. Briefs*, vol. 59, no. 4, pp. 234–238, Apr. 2012.

[33] S. Wang, T. J. Koickal, A. Hamilton, R. Cheung, and L. S. Smith, "A bio-realistic analog CMOS cochlea filter with high tunability and ultra-steep roll-off," *IEEE Trans. Biomed. Circuits Syst.*, vol. 9, no. 3, pp. 297–311, Jun. 2015.

[34] K. M. H. Badami, S. Lauwereins, W. Meert, and M. Verhelst, "A 90 nm CMOS, 6 μW power-proportional acoustic sensing frontend for voice activity detection," *IEEE J. Solid-State Circuits*, vol. 51, no. 1, pp. 291–302, Jan. 2016.

[35] C. Trigona, B. Andò, S. Baglio, R. L. Rosa, and G. Zoppi, "Sensors for kinetic energy measurement operating on 'zero-current standby'," *IEEE Trans. Instrum. Meas.*, vol. 66, no. 4, pp. 812–820, Apr. 2017.

[36] M. D. Prieto, D. Z. Millan, W. Wang, A. M. Ortiz, J. A. O. Redondo, and L. R. Martinez, "Self-powered wireless sensor applied to gear diagnosis based on acoustic emission," *IEEE Trans. Instrum. Meas.*, vol. 65, no. 1, pp. 15–24, Jan. 2016.

[37] R. Hussein, K. B. Shaban, and A. H. El-Hag, "Robust feature extraction and classification of acoustic partial discharge signals corrupted with noise," *IEEE Trans. Instrum. Meas.*, vol. 66, no. 3, pp. 405–413, Mar. 2017.

[38] J. Huang, X. Zhang, F. Guo, Q. Zhou, H. Liu, and B. Li, "Design of an acoustic target classification system based on small-aperture microphone array," *IEEE Trans. Instrum. Meas.*, vol. 64, no. 7, pp. 2035–2043, Jul. 2015.

[39] Q. Zhao, M. Ji, R. Li, and Z. J. Ren, "Long-term performance of sediment microbial fuel cells with multiple anodes," *Bioresource Technol.*, vol. 237, pp. 178–185, Aug. 2017.

[40] R. Shannon. *Implementation of the MudWatt Microbial Fuel Cell*. Accessed: Oct. 10, 2018. [Online]. Available: http://www.fuelcellstore.com/downloads/mfc/mudwatt-101-an-intro-mfcs.pdf

[41] Invensense. *Invensense: Microphone Specifications Application Note AN-1112*. Accessed: Oct. 10, 2018. [Online]. Available: http://www.invensense.com/wp-content/uploads/2015/02/AN-1112-v1.1.pdf

[42] J. Eargle, *The Microphone Book*. Waltham, MA, USA: Focal Press, 2004.

[43] *San Francisco Maritime National Park Association Dataset*. Accessed: Oct. 10, 2018. [Online]. Available: https://maritime.org/sound/

Philipp Mayer (S'17) received the B.Sc. degree in electrical engineering and information technology from TU Wien, Vienna, Austria, in 2016, and the M.Sc. degree from ETHZ, Zurich, Switzerland, in 2018, where he is currently pursuing the Ph.D. degree with the Integrated System Laboratory.

His research interests include low-power system design, energy harvesting, wireless optogenetics, and edge computing.

Michele Magno (SM'13) received the master's and Ph.D. degrees in electronic engineering from the University of Bologna, Bologna, Italy, in 2004 and 2010, respectively.

He is currently a Post-Doctoral Researcher with ETH Zürich, Zürich, Switzerland, and a Research Fellow with the University of Bologna. He has authored over 100 papers in international journals and conferences. His research interests include wireless sensor networks, wearable devices, energy harvesting, low power management techniques, and extension of lifetime of battery-operating devices.

Luca Benini (F'03) holds the Chair of digital Circuits and systems with ETHZ and is a Full Professor at the Universita di Bologna, Bologna, Italy. He is active in the design ultra-low-power VLSI Circuits and smart sensing microsystems. He has authored more than 900 peer-reviewed papers and five books. His research interests include energy-efficient computing systems design, from embedded to high performance.

Mr. Benini is a fellow of the ACM and a member of the Academia Europaea. He was a recipient of the 2016 IEEE CAS Mac Van Valkenburg Award.